Mixed Convective Magnetohydrodynamic Peristaltic Flow of a Jeffrey Nanofluid with Newtonian Heating

Noreen Sher Akbar[a] and Sohail Nadeem[b]

[a] DBS&H, CEME, National University of Sciences and Technology, Islamabad, Pakistan
[b] Department of Mathematics, Quaid-i-Azam University 45320, Islamabad 44000, Pakistan

Reprint requests to N. S. A.; E-mail: noreensher@yahoo.com

Z. Naturforsch. **68a,** 433 – 441 (2013) / DOI: 10.5560/ZNA.2013-0029
Received December 10, 2012 / revised January 31, 2013 / published online May 22, 2013

We present the mixed convective peristaltic motion of a magnetohydrodynamic (MHD) Jeffrey nanofluid in an asymmetric channel with Newtonian heating. In the peristaltic literature, Newtonian heating is used for the first time in the present article. The peristaltic flow of a nanofluid with Newtonian heating is not explored so far. So in the present problem, first we model the mixed convective peristaltic motion of a MHD Jeffrey nanofluid in an asymmetric channel with Newtonian heating. According to the realistic approch, the problem formulation is made under long wavelength and low Reynolds number approximation. We get the four coupled equations. Homotopy perturbation method (HPM) solutions are calculated for nanoparticle fraction and heat transfer phenomena, while exact solutions are evaluated for stream function and pressure gradient. The possessions of different parameters on the flow quantities of observation are analyzed graphically and physically. In the end, the streamlines are plotted and discussed.

Key words: Peristaltic Flow; Asymmetric Channel; Jeffrey Nanofluid; Newtonian Heating.

1. Introduction

Peristaltic motion is an important mechanism for transporting fluids. This phenomenon usually occurs when the cross-section of an artery or a muscle contracts and expands periodically by the progression of a progressive wave. Peristaltic motion happens generally when a stenosis is created in the functioning of ureter, chyme movement in intestine, movement of egg in fallopian tube, the transport of spermatozoa in the cervical canal, transport of bile in bile duct, transport of cilia etc. Muthu et al. [1] investigated the effects of viscoelastic wall properties and micropolar fluid parameters on the flow with deformable boundaries. Peristaltic transport of a Newtonian fluid through a uniform and a non-uniform annulus is developed by Mekheimer [2]. In another article, Mekheimer [3] discussed the effect of the induced magnetic field on the peristaltic flow of a couple stress fluid in a channel. Sanyal and Biswas [4] presumed blood to be an incompressible viscous Newtonian fluid to discuss two-dimensional peristaltic motions through a circular tube. Some important articles describing the features of peristaltic flows are cited in [5 – 8].

Nanofluids are fluids exhibiting advanced thermal properties, having higher thermal conductivity and heat transfer coefficients as compared to the base fluid. They have been widely deliberated for improved thermal properties. The involvement of nanofluids with improved heat uniqueness can be remarkable in conditions of more competent cooling systems, consequential effecting higher productivity and energy savings. Several prospective applications for nanofluids are heat exchangers, radiators for engines, process cooling systems, microelectronics, etc. The idea of nanofluid was first given by Choi [9]. Later on Buongiorno [10], Sadik and Pramuanjaroenkij [11] and Marga et al. [12] analyzed the convective heat transfer enhancement with nanofluids. The Cheng–Minkowycz problem for a natural convective boundary-layer flow saturated by a nanofluid is discussed by Nield and Kuznetsov [13, 14]. In another article, Kuznetsov and Nield [15] presented a natural convective boundary-layer flow of a nanofluid past a vertical plate. Khan and Pop [16] give the first article for the boundary-layer flow of a nanofluid past a stretching sheet. Peristaltic flow with nanofluids was first discussed by Akbar and Nadeem [17] and Akbar

et al. [18]. Some other important references are cited in [19–21].

Newtonian heating is a heating where the heat transfer rate from the bounding surface with a finite heat capacity is proportional to the local surface temperature and which is usually termed conjugate convective flow [22]. This type of heating on the peristaltic flow is useful due to its practical applications in hemodylasis and oxygenation, in obtaining information about the properties of tissues, in hypothermia treatment, sanitary fluid transport, blood pump in heart lungs machine, and transport of corrosive fluids. Pop et al. [23] discussed the asymptotic solutions for the free convection boundary layer flow along a vertical surface in a porous medium with Newtonian heating. Effects of partial slip, viscous dissipation, and Joule heating on Von Kármán flow and heat transfer of an electrically conducting non-Newtonian fluid is presented by Sahoo [24]. Boundary layer flow and heat transfer over a stretching sheet with Newtonian heating is taken into account by Salleh et al. [25].

Here we have the first article in the peristaltic literature which gives the Jeffrey nanofluid with Newtonian heating in an asymmetric channel. The homotopy perturbation method (HPM) gives the solutions for nanoparticle fraction and heat transfer for the developed problem, while exact solutions are constructed for stream function and pressure gradient. Graphical discussion and physical behaviour of the conjugate parameter for Newtonian heating γ_t, Hartman number M, thermophoresis parameter N_t, Brownian motion parameter N_b, Jeffrey fluid Parameter λ_1, and amplitudes are presented. Main results are given at the end of the article.

2. Formulation of Flow Equations

Here we present an incompressible MHD Jeffrey nanofluid with Newtonian heating in an asymmetric channel with channel width d_1+d_2, and a sinusoidal wave propagating with constant speed c along the walls of the channel. Asymmetry in the channel flow is retained due to the following wall surfaces expressions:

$$\begin{aligned} Y &= H_1 = d_1 + a_1 \cos\left[\frac{2\pi}{\lambda}(X-ct)\right], \\ Y &= H_2 = -d_2 - b_1 \cos\left[\frac{2\pi}{\lambda}(X-ct)+\phi\right]. \end{aligned} \tag{1}$$

In the above equations, a_1 and b_1 denote the wave amplitudes, λ is the wave length, d_1+d_2 the channel width, c the wave speed and t the time. X is the direction of wave propagation, and Y is perpendicular to X. The expression for fixed and wave frames are related by the following relations:

$$\begin{aligned} &\bar{x} = \bar{X} - ct\,,\ \ \bar{y} = \bar{Y}\,,\ \ \bar{u} = \bar{U} - c \\ &\bar{v} = \bar{V}\,,\ \ p(x) = P(\bar{X},t)\,. \end{aligned} \tag{2}$$

The Jeffrey fluid model is defined by

$$S = \frac{\mu}{1+\lambda_1}(\dot{\gamma} + \lambda_2 \ddot{\gamma})\,. \tag{3}$$

In above equation, μ is the viscosity, λ_1 the ratio of relaxation to retardation times, $\dot{\gamma}$ the shear rate, λ_2 the retardation time, and dots denote the differentiation with respect to time. We introduce the following non-dimensional quantities:

$$\begin{aligned} &x = \frac{2\pi\bar{x}}{\lambda}\,,\ \ y = \frac{\bar{y}}{d_1}\,,\ \ u = \frac{\bar{u}}{c_1}\,, \\ &v = \frac{\bar{v}}{c_1}\,,\ \ t = \frac{2\pi\bar{t}}{\lambda}\,,\ \ \delta = \frac{2\pi d_1}{\lambda}\,, \\ &d = \frac{d_2}{d_1}\,,\ \ P = \frac{2\pi d_1^2 P}{\mu c_1 \lambda}\,,\ \ h_1 = \frac{\bar{h}_1}{d_1}\,, \\ &h_2 = \frac{\bar{h}_2}{d_2}\,,\ \ \mathrm{Re} = \frac{\rho c_1 d_1}{\mu}\,,\ \ a = \frac{a_1}{d_1}\,, \\ &b = \frac{a_2}{d_1}\,,\ \ d = \frac{d_2}{d_1}\,,\ \ S = \frac{\bar{S} d_1}{\mu c_1}\,, \\ &\theta = \frac{\bar{T}-\bar{T}_0}{\bar{T}_1-\bar{T}_0}\,,\ \ \sigma = \frac{\bar{C}-\bar{C}_0}{\bar{C}_1-\bar{C}_0}\,, \\ &\alpha = \frac{k}{(\rho c)_f}\,,\ \ N_b = \frac{(\rho c)_p D_B(\bar{C}_1-\bar{C}_0)}{(\rho c)_f \alpha}\,, \\ &\mathrm{Pr} = \frac{\nu}{\alpha}\,,\ \ N_t = \frac{(\rho c)_p D_{\bar{T}}(\bar{T}_1-\bar{T}_0)^2}{\bar{T}_0(\rho c)_f \alpha}\,, \\ &\mathrm{Gr} = \frac{g\alpha d_1^2(\bar{T}_1-\bar{T}_0)}{\nu c_1}\,,\ \ \mathrm{Br} = \frac{g\alpha d_1^2(\bar{C}_1-\bar{C}_0)}{\nu c_1}\,, \end{aligned} \tag{4}$$

where Pr, N_b, N_t, Gr, and Br, denote respectively the Prandtl number, the Brownian motion parameter, the thermophoresis parameter, the local temperature Grashof number, and the local nanoparticle Grashof number.

Stream function and velocity field are related by the expressions

$$u = \frac{\partial \Psi}{\partial y}\ \ v = -\delta \frac{\partial \Psi}{\partial x}\,. \tag{5}$$

With the help of (3) – (5) under the the long wavelength and low Reynolds number assumption, we have the following equations:

$$\frac{1}{1+\lambda_1}\frac{\partial^4\Psi}{\partial y^4} - M^2\frac{\partial^2\Psi}{\partial y^2} + \mathrm{Gr}\frac{\partial\theta}{\partial y} + \mathrm{Br}\frac{\partial\sigma}{\partial y} = 0\,, \tag{6}$$

$$\frac{\mathrm{d}P}{\mathrm{d}x} = \frac{\partial}{\partial y}\left[\frac{1}{1+\lambda_1}\frac{\partial^2\Psi}{\partial y^2} - M^2\right] + \mathrm{Gr}\theta + \mathrm{Br}\sigma\,, \tag{7}$$

$$\frac{\partial^2\theta}{\partial y^2} + N_\mathrm{b}\frac{\partial\theta}{\partial y}\frac{\partial\sigma}{\partial y} + N_\mathrm{t}\left(\frac{\partial\theta}{\partial y}\right)^2 = 0\,, \tag{8}$$

$$\frac{\partial^2\sigma}{\partial y^2} + \frac{N_\mathrm{t}}{N_\mathrm{b}}\left(\frac{\partial^2\theta}{\partial y^2}\right) = 0\,. \tag{9}$$

The non-dimensionaless boundary conditions are

$$\Psi = \frac{F}{2}\,,\ \frac{\partial\Psi}{\partial y} = -1\,,\ \theta'(h_1) + \gamma_i\theta(h_1) = -\mathrm{Bi}\,, \tag{10a}$$
$$\sigma = 1 \ \text{ at } \ y = h_1 = 1 + a\cos x\,,$$

$$\Psi = -\frac{F}{2}\,,\ \frac{\partial\Psi}{\partial y} = -1\,,\ \theta = 0\,, \tag{10b}$$
$$\sigma = 0 \ \text{ at } \ y = h_2 = -d - b\cos(x+\phi)\,,$$

where $\gamma = h_s d_1$ is the conjugate parameter for Newtonian heating, and h_s is the heat transfer parameter.

The flow rates in fixed and wave frame are related by

$$Q = F + 1 + d\,. \tag{11}$$

3. Flow Profiles

Adopting the procedure done by [17, 18], the solution expressions for stream function, temperature profile, nanoparticle fraction, and pressure gradient can be written as

$$\begin{aligned}\Psi(x,y) &= H_{10}y^2 + H_{11}y^3 + H_{27}y + H_{26}\\ &+ H_{24}\left(\cosh\left(\sqrt{M^2(1+\lambda)}y\right) + \sinh\left(\sqrt{M^2(1+\lambda)}y\right)\right)\\ &\cdot\left(M^2(1+\lambda)\right)^{-1} H_{25}\left(\cosh\left(\sqrt{M^2(1+\lambda)}y\right)\right.\\ &\left.-\sinh\left(\sqrt{M^2(1+\lambda)}y\right)\right)\left(M^2(1+\lambda)\right)^{-1},\end{aligned} \tag{12}$$

$$\begin{aligned}\frac{\mathrm{d}P}{\mathrm{d}x} &= \Big((1+H_{15})H_{17}H_{20} - (1+H_{15})H_{19}H_{20}\\ &- H_{16}H_{21} - H_{15}H_{16}H_{21} + H_{18}H_{21} + H_{15}H_{18}H_{21}\\ &\cdot(1+H_{14})H_{17}H_{22} + (1+H_{15})H_{19}H_{22} + H_{12}H_{22}H_{21}\\ &+ H_{16}H_{23} - H_{13}H_{21}H_{22} + H_{16}H_{12} + H_{14}H_{16}H_{23}\\ &- H_{18}H_{23} - H_{14}H_{18}H_{23} - H_{12}H_{20}H_{23}\\ &+ H_{13}H_{20}H_{23} - H_{21}H_{22}F + H_{20}H_{23}F\Big)\Big(H_{19}(H_{20}\\ &- H_{22}) + H_{17}(-H_{20} + H_{22}) + (H_{16} - H_{18})(H_{21} - H_{23})\\ &- (H_{21}H_{22} - H_{20}H_{23})(h_1 - h_2)\Big)^{-1},\end{aligned} \tag{13}$$

$$\begin{aligned}\theta(x,y) &= \frac{2\gamma(h_2 - y)}{1+\gamma(h_1 - h_2)} - \frac{\gamma N_\mathrm{b} y^2}{2(h_1 - h_2)(1+\gamma(h_1 - h_2))}\\ &+ H_1 y + H_2\,,\end{aligned} \tag{14}$$

$$\begin{aligned}\sigma(x,y) &= \frac{(h_2 - y)}{(h_2 - h_1)} - \frac{N_\mathrm{t}}{N_\mathrm{b}}\left(\frac{\gamma(h_2 - y)}{1+\gamma(h_1 - h_2)}\right.\\ &- \frac{\gamma N_\mathrm{b} y^2}{2(h_1 - h_2)(1+\gamma(h_1 - h_2))}\\ &\left.+ H_1 y + H_2\right) + H_3 y + H_4\,,\end{aligned} \tag{15}$$

where $H_1 - H_{27}$ are constants evaluated using Mathematica 8.

The dimensionless pressure rise ΔP is defined by

$$\Delta P = \int_0^1 \left(\frac{\mathrm{d}P}{\mathrm{d}x}\right)\mathrm{d}x\,. \tag{16}$$

4. Graphical Illustration

In this section, we present the pressure rise, pressure gradient, velocity, temperature profile, nanoparticle fraction, and streamlines for Biot number Bi, Hartman number M, thermophoresis parameter N_t, Brownian motion parameter N_b, local temperature Grashof number Gr, relaxation time λ_1, and conjugate parameter for Newtonian heating γ through graphs. Numerical integration is performed for the pressure rise per wavelength. The pressure rise against volume flow rate is illustrated in Figures 1a to 1e. It is noticed that the pressure rise and volume flow rate have opposite behaviours. From Figures 1a to 1e it is found that in the pumping region ($\Delta P > 0$), the pressure rise decreases with the increase in Hartman number M, conjugate parameter for Newtonian heating γ, and relaxation time λ_1 while the pressure rise increases with the increase in thermophoresis parameter N_t and local temperature Grashof number Gr. Figures 1a and 1e also show that in the augmented pumping region for ($\Delta P < 0$), the pressure rise gives the opposite results for all parameters as compared to the pumping region ($\Delta P > 0$). Free

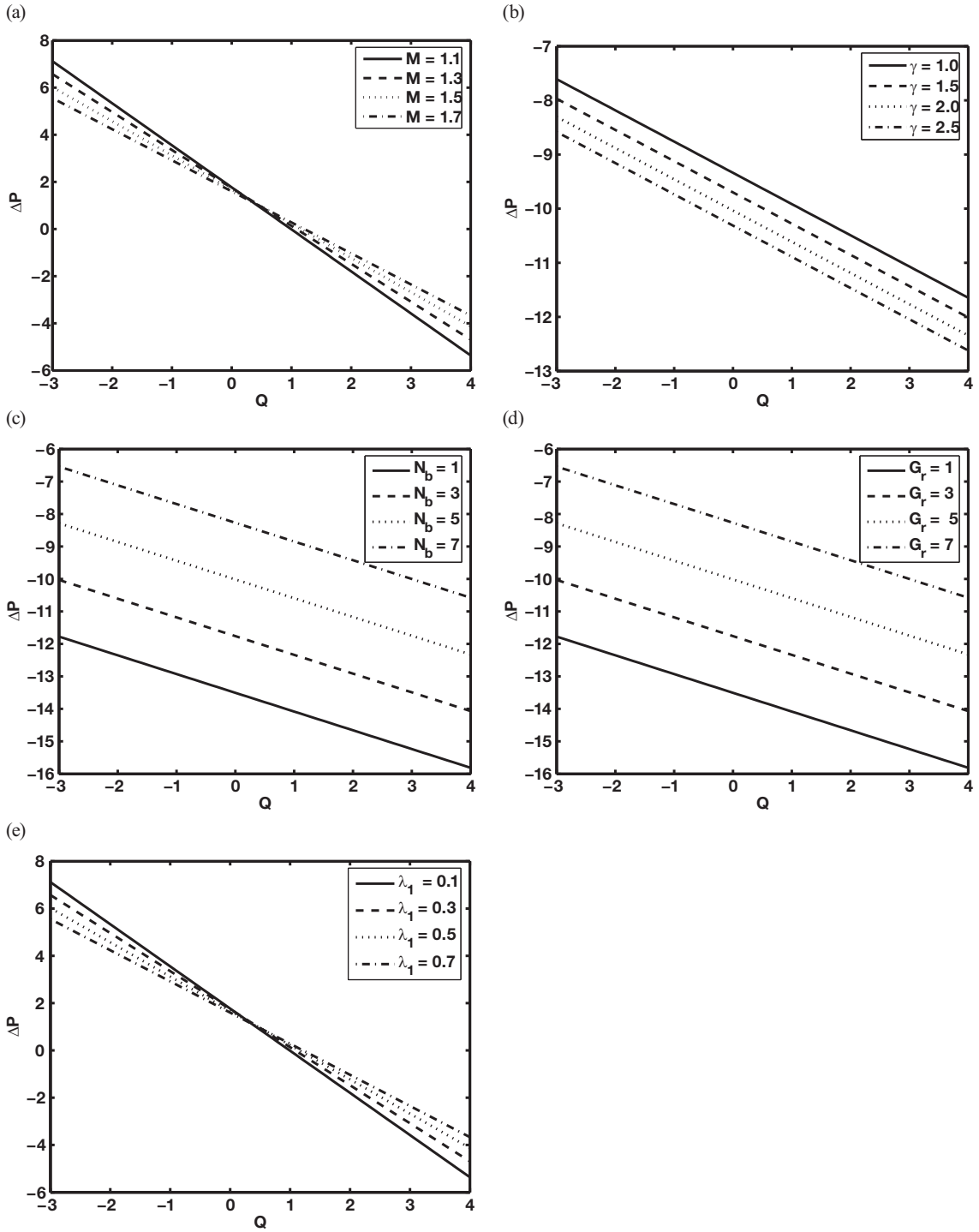

Fig. 1. Pressure rise for (a) $N_t = 2$, $\gamma = 2$, $\lambda_1 = 0.5$, and Gr $= 2$; (b) $M = 0.5$, $\lambda_1 = 0.5$, $N_b = 2$, and Gr $= 2$; (c) $\lambda_1 = 0.5$, $M = 0.5$, Gr $= 2$, and $\gamma = 2$; (d) $N_b = 2$, $\gamma = 2$, $M = 0.5$, and $M = 2$; (e) $N_b = 2$, $\gamma = 2$, Gr $= 0.5$, and $M = 2$. Other parameters are $d = 1$, $\phi = 0.2$, Br $= 2$, $a = 0.4$, $N_t = 0.4$, and $b = 0.2$.

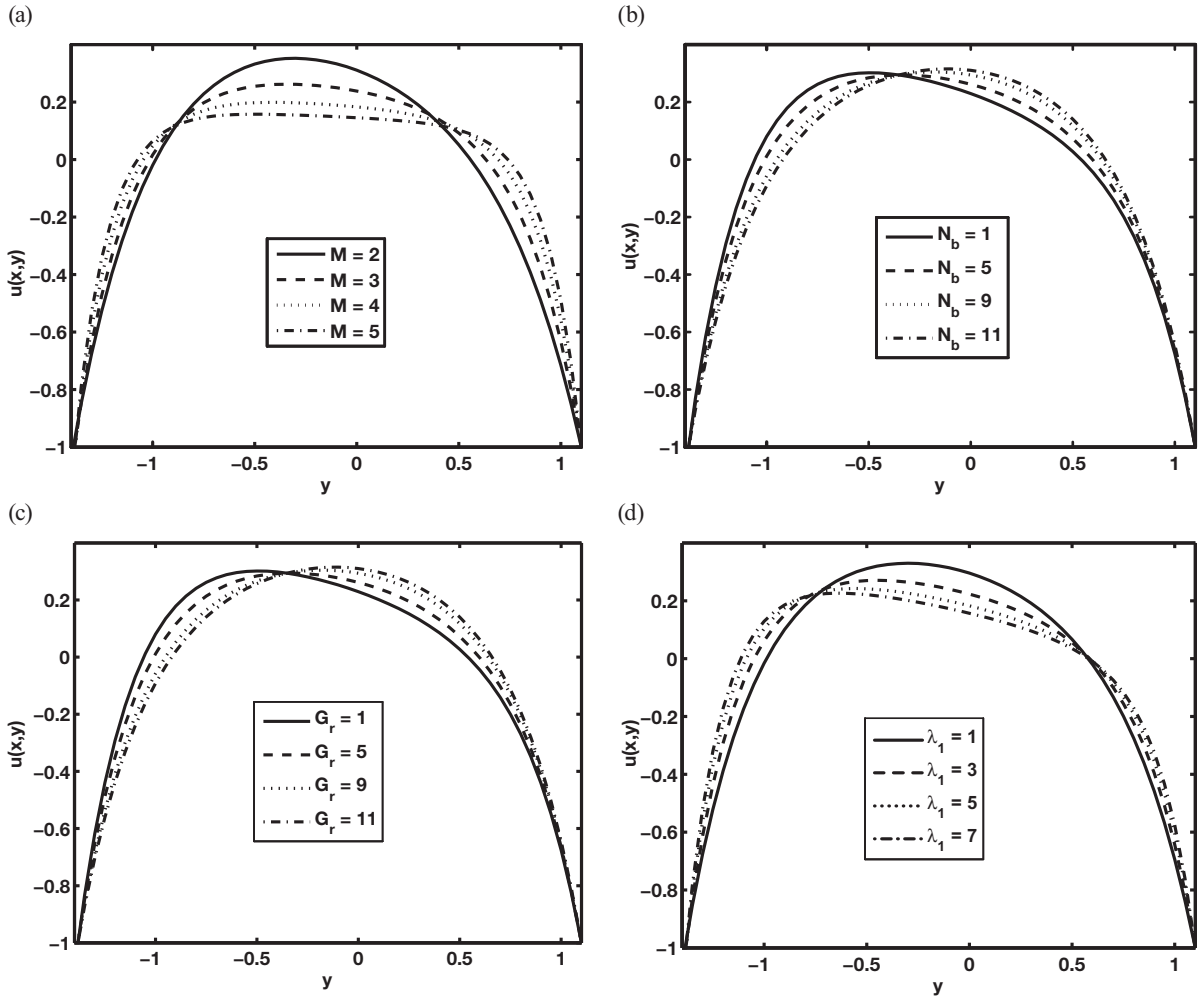

Fig. 2. Velocity profile for (a) $\mathrm{Gr} = 2$, $\lambda_1 = 0.5$, and $N_\mathrm{b} = 2$; (b) $M = 2$, $\mathrm{Gr} = 2$, and $\lambda_1 = 2$; (c) $M = 2$, $\lambda_1 = 0.5$, and $N_\mathrm{b} = 2$; (d) $N_\mathrm{b} = 0.5$, $\mathrm{Gr} = 2$, and $M = 2$. Other parameters are $a = 0.1$, $x = 1$, $d = 1$, $\phi = 0.7$, $b = 0.5$, $\mathrm{Br} = 2$, $N_\mathrm{t} = 2$, $Q = 2$, and $\gamma = 2$.

pumping region holds when $(\Delta P = 0)$. Variations of Hartman number M, relaxation time λ_1, Grashof number Gr, and Brownian motion parameter N_b on the velocity profile are shown in Figures 2a to 2d. Figure 2a depicts that the behaviour of the velocity near the channel walls and at the center are not similar in view of the Hartman number M. The velocity field increases due to an increase in M near the channel walls while the velocity field decreases at the centre of the channel. The velocity for the Brownian motion parameter N_b, relaxation time λ_1, and Grashof number Gr is plotted in Figures 2b, c, and d. Here the behaviour of the velocity field in view of relaxation time λ_1 and Grashof number Gr is not same in qualitative sense as compared to the behaviour of relaxation time λ_1 and Brownian motion parameter N_b.

The pressure gradients for different values of M, γ, Gr, and N_b are plotted in Figures 3a to 3d. The magnitude of pressure gradient increases with the increase in M, γ, Gr, and N_b. It is also observed that the maximum pressure gradient occurs when $x = 0.48$, and the pressure gradient near the channel walls is small. This leads to the fact that flow can easily pass in the middle of the channel.

Variations of temperature profile for different values of conjugate parameter for Newtonian heating γ and Brownian motion parameter N_b are displayed in Figures 4a and 4b. It is seen through Figure 4a

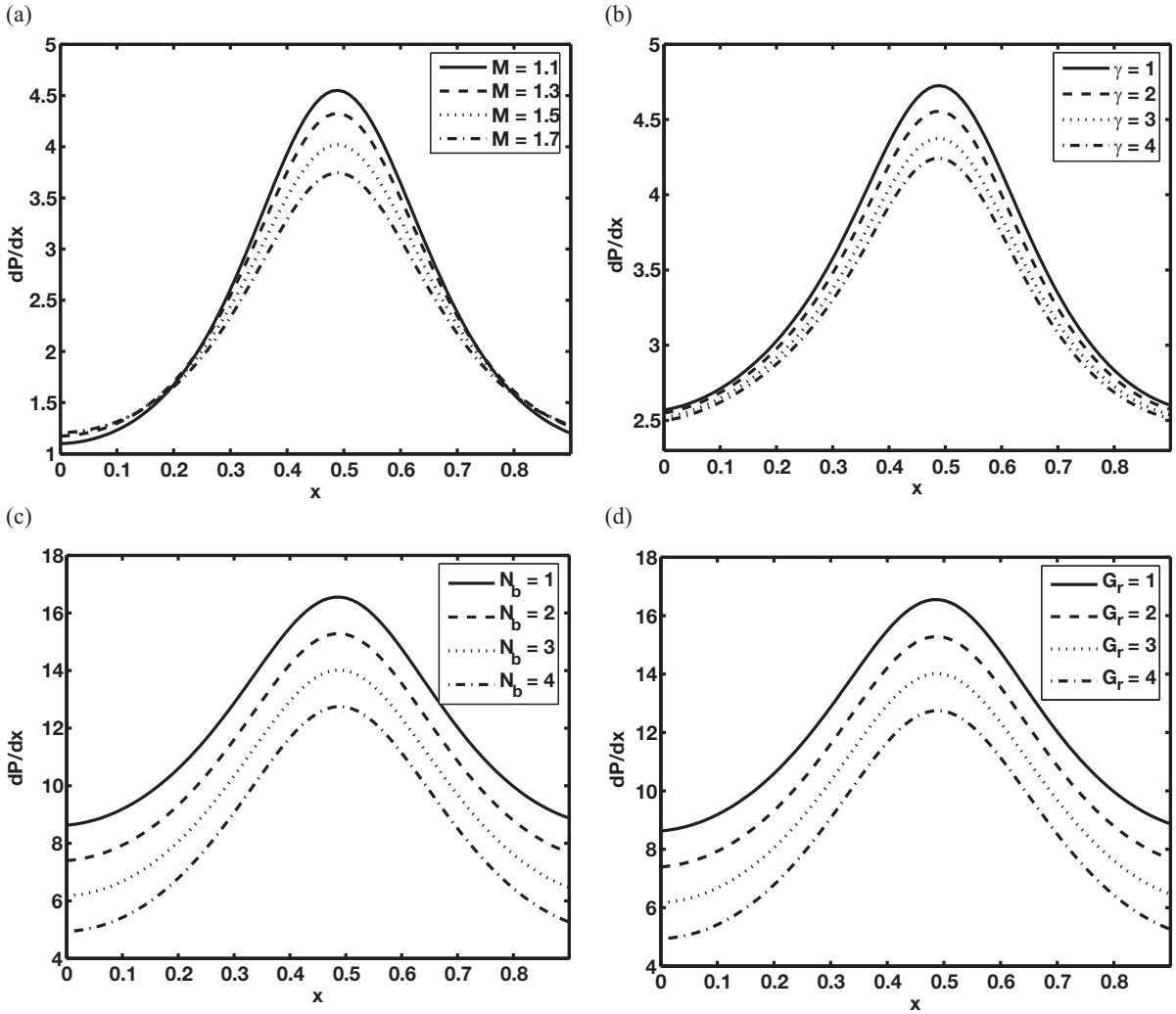

Fig. 3. Pressure gradient for (a) Bi = 2, Gr = 2, and $N_b = 0.4$; (b) $M = 2$, Gr = 2, and $N_b = 0.4$; (c) $\gamma = 2$, $M = 2$, and Gr = 0.5; (d) $\gamma = 2$, $N_b = 0.5$, and $M = 2$. Other parameters are $\lambda_1 = 0.5$, $a = 0.4$, $Q = -1$, $d = 1$, $\phi = 0.2$, $b = 0.2$, Br = 2, and $N_t = 2$.

and b that when we increase the conjugate parameter for Newtonian heating γ and the Brownian motion parameter N_b, the temperature profile increases. Figure 5a and b depicts the nanoparticle fraction for different values of the conjugate parameter for Newtonian heating γ and the thermophoresis parameter N_t. It is analyzed that when we increase the conjugate parameter for Newtonian heating γ and the thermophoresis parameter N_t, the nanoparticle fraction increases.

The trappings for different values of λ_1, Gr, and N_t are shown in Figures 6a to 6f. It is seen from Figures 6a and b that with the increase in the value of λ_1, the size of the trapping bolus increases (in the second and third quadrant). Streamlines for different values of Gr have been plotted in Figure 6c and d. It is found that with an increase in Gr, the size of the trapping bolus increases, and the number of the trapping bolus decreases (in all quadrants). Figures 6e and f depict that with the increase in the value of N_t, the size of the trapping bolus decreases (in the second and fourth quadrant) while in the first and third quadrant size and number of the trapping bolus decreases.

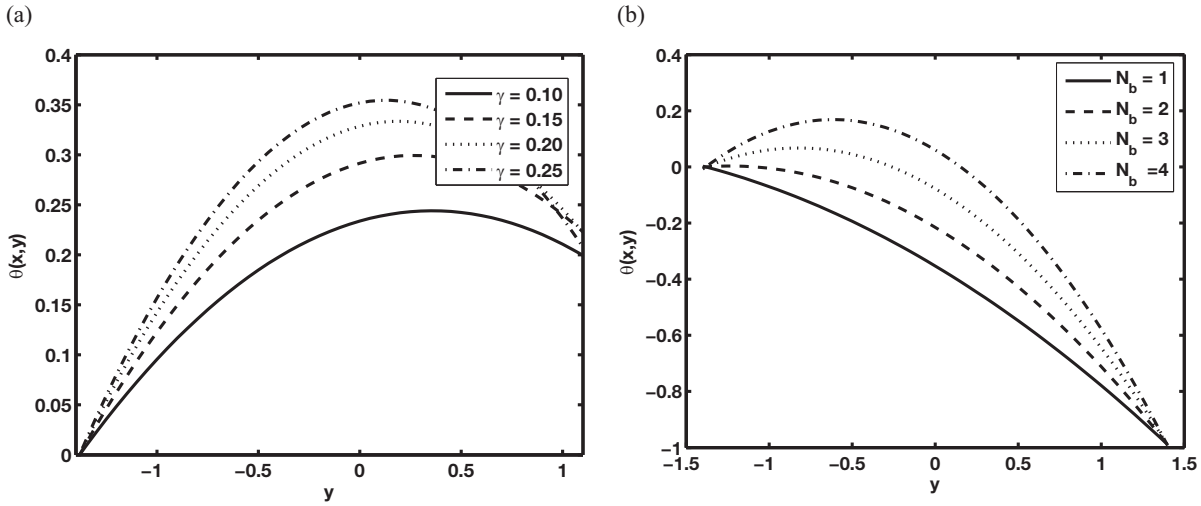

Fig. 4. Temperature profile for (a) $N_b = 0.4$; (b) $\gamma = 2$. Other parameters are $a = 0.1$, $x = 1$, $d = 1$, $\phi = 0.7$, $b = 0.5$, and $N_t = 2$.

5. Conclusions

We have presented the mixed convective peristaltic motion of a MHD Jeffrey nanofluid in an asymmetric channel with Newtonian heating. The main points of the current study are as follows.

i. It is noticed that the pressure rise and volume flow rate have opposite behaviours.

ii. It is found that in the pumping region the pressure rise decreases with the increase in Hartman number M, conjugate parameter for Newtonian heating γ, and relaxation time λ_1 while the pressure rise increases with the increase in thermophoresis parameter N_t and local temperature Grashof number Gr.

iii. It depicts that the behaviour of the velocity near the channel walls and at the center are not similar

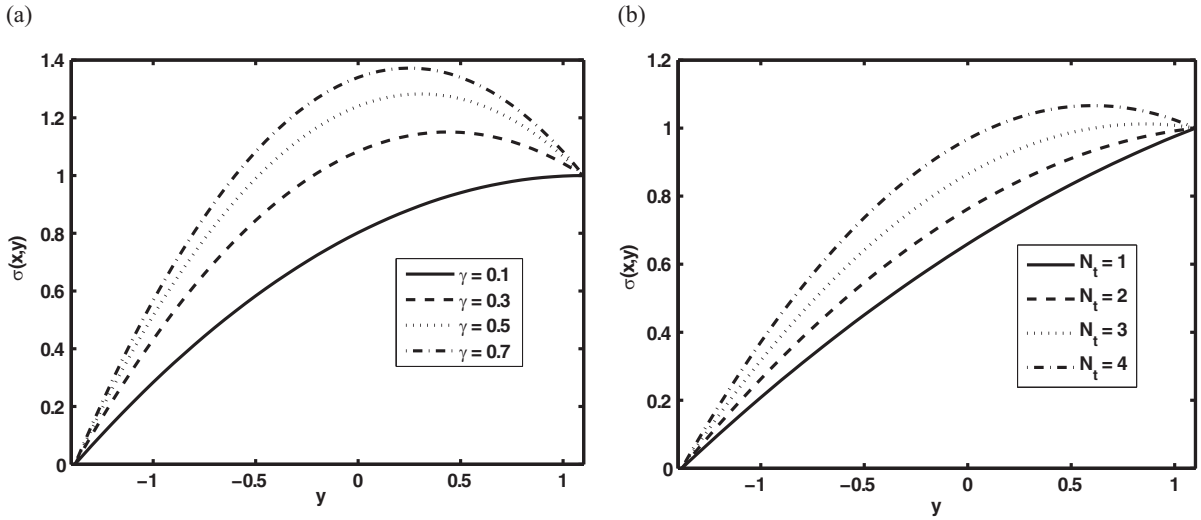

Fig. 5. Nanoparticle fraction for (a) $N_t = 0.4$; (b) $\gamma = 2$. Other parameters are $a = 0.1$, $x = 1$, $d = 1$, $\phi = 0.7$, $b = 0.5$, and $N_b = 2$.

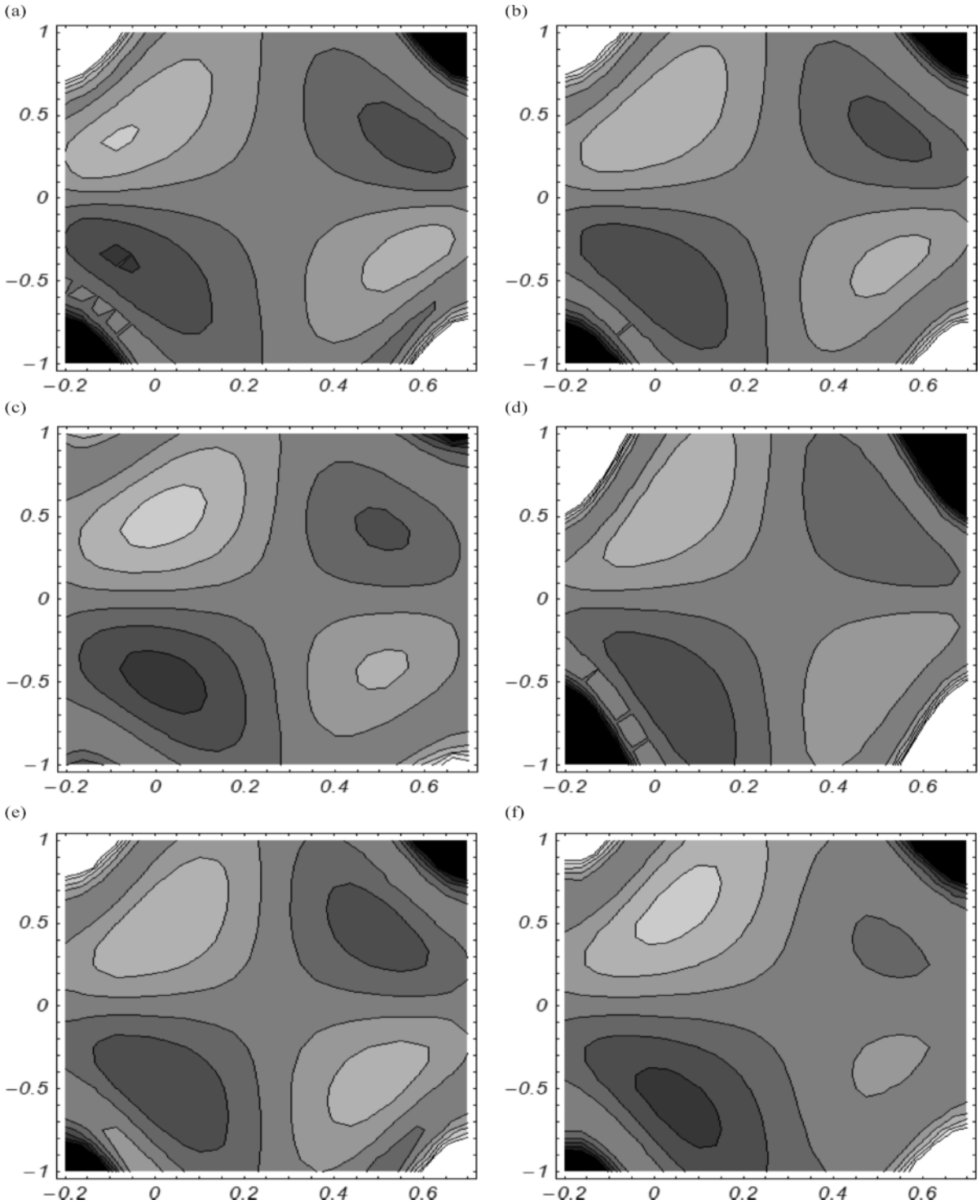

Fig. 6. Streamlines for panels (a) and (b), where $\lambda_1 = 0.4, 0.6$; (c) and (d) for $\mathrm{Gr} = 2, 3$; (e) and (f) for $N_\mathrm{t} = 0.2, 0.6$. Other parameters are $Q = 2$, $a = 0.1$, $x = 1$, $d = 1$, $\phi = 0.7$, $b = 0.5$, $\mathrm{Br} = 2$, $N_\mathrm{b} = 2$, and $\gamma = 2$.

in view of the Hartman number M. The velocity field increases due to an increase in M near the channel walls while the velocity field decreases at the centre of the channel.

iv. Here the behaviour of the velocity field in view of relaxation time λ_1 and Grashof number Gr is not the same in a qualitative sense as compared to the behaviour of relaxation time λ_1 and Brownian motion parameter N_b.

v. The magnitude of pressure gradient increases with the increase in M, γ, Gr, and N_b.

vi. When we increase the conjugate parameter for Newtonian heating γ and the Brownian motion parameter N_b, the temperature profile increases.

vii. It is analyzed that when we increase the conjugate parameter for Newtonian heating γ and the thermophoresis parameter N_t, the nanoparticle fraction increases.

viii. With an increase in Gr, the size of the trapping bolus increases and the number of the trapping bolus decreases (in all quadrants).

ix. It is found that with the increase in the value of N_t, the size of the trapping bolus decreases (in the second and fourth quadrant) while in the first and third quadrant, size and number of the trapping bolus decreases.

x. It is observed that with the increase in the value of λ_1, the size of the trapping bolus increases (in the second and third quadrant).

[1] P. Muthu, B. V. R. Kumar, and P. Chandra, ANZIAM J. **41**, 245 (2003).
[2] Kh. Mekheimer, Arab. J. Sci. Eng. **30**, 69 (2005).
[3] Kh. S. Mekheimer, Phys. Lett. A. **372**, 4271 (2008).
[4] D. C. Sanyal and A. Biswas, Bull. Soc. Math. **17**, 43 (2010).
[5] J. C. Mishra and S. Maiti, J. Mech. Med. Biol. **2**, 1108 (2011).
[6] D. Tripathi, S. K. Pandey, and S. Das, Appl. Math. Comp. **215**, 3645 (2010).
[7] D. Tripathi, Math. Biosci. **233**, 90 (2011).
[8] N. S. Akbar, S. Nadeem, T. Hayat, and S. Obaidat, Int. J. Heat Mass Trans. **55**, 1855 (2012).
[9] S. U. S. Choi, ASME **66**, 99 (1995).
[10] J. Buongiorno, J. Heat Trans. **128**, 240 (2010).
[11] K. Sadik and A. Pramuanjaroenkij, Int. J. Heat Mass Trans. **52**, 3187 (2009).
[12] S. E. B. Marga, S. J. Palm, C. T. Nguyen, G. Roy, and N. Galanis, Int. J. Heat Fluid Flow **26**, 530 (2005).
[13] D. A. Nield and A. V. Kuznetsov, Int. J. Heat Mass Trans. **52**, 5792 (2009).
[14] D. A. Nield and A. V. Kuznetsov, Int. J. Heat Mass Trans. **54**, 374 (2011).
[15] A. V. Kuznetsov and D. A. Nield, Int. J. Therm. Sci. **49**, 243 (2010).
[16] W. A. Khan and I. Pop, Int. J. Heat Mass Trans. **53**, 2477 (2010).
[17] N. S. Akbar and S. Nadeem, Commun. Theor. Phys. **56**, 761 (2011).
[18] N. S. Akbar, S. Nadeem, T. Hayat, and A. A. Hendi, Heat Mass Trans. **48**, 451 (2012).
[19] A. Zeeshan, R. Ellahi, A. M. Siddiqui, and H. U. Rahman, Int. J. Phys. Sci. **7**, 1353 (2012).
[20] R. Ellahi, Appl. Math. Model. **37**, 1451 (2013).
[21] R. Ellahi, M. Raza, and K. Vafai, Math. Comput. Model. **55**, 1876 (2012).
[22] D. Lesnic, D. B. Ingham, I. Pop, and C. Storr, Heat Mass Trans. **40**, 665 (2004).
[23] I. Pop, D. Lesnic, and D. B. Ingham, Hyb. Meth. Eng. **2**, 132 (2000).
[24] B. Sahoo, Commun. Nonlin. Sci Numer. Simul. **14**, 2982 (2009).
[25] M. Z. Salleh, R. Nazar, and I. Pop, J. Taiwan Inst. Chem. Eng. **41**, 651 (2010).